Progress In Electromagnetics Research B, Vol. 15, 151–173, 2009

PROPAGATION, EXCITATION, AND ORTHOGONALITY OF MODES IN A PARALLEL PLATE, ANISOTROPIC WAVEGUIDE USING A MODIFIED, COORDINATE TRANSFORMATION

J. M. Jarem

Electrical and Computer Engineering Department
University of Alabama in Huntsville
Huntsville, AL, USA

Abstract—The excitation of forward and backward, Electromagnetic (EM) modes and fields in an anisotropic, parallel plate waveguide (meeting Dirichlet and Neumann boundary conditions), is studied, using a modified coordinate transformation which reduces Maxwell's equations to the form of a Helmholtz wave equation satisfying Dirichlet and mixed-partial derivative boundary conditions. The EM modes and fields of the system are excited by a novel, slanted electric surface current excitation whose slant angle has been chosen to coincide with the surfaces of constant phase of the anisotropic modes which may propagate in the waveguide. Also presented in the paper, for comparison purposes, is the EM field excitation analysis corresponding to an isotropic parallel plate waveguide whose waveguide characteristics are close to those of the anisotropic waveguide. Several results are presented herein, including; a novel waveguide modal characteristic equation analysis used to determine the propagating and complex (or non propagating) modes that may exist in an anisotropic waveguide system, a novel study of backward-forward modal orthogonality based on the complex Poynting theorem and a power-energy reaction integral equation, descriptions of the matrix analyses used to determine the EM fields excited in the anisotropic and isotropic waveguide systems under consideration, and several numerical results.

Corresponding author: J. M. Jarem (jarem@eng.uah.edu).

1. INTRODUCTION

An important problem in electromagnetics consists of determining the propagation, excitation, power characteristics and Green's functions that occur in a layered waveguide system containing anisotropic or bianisotropic media [1–7]. This problem is important in such areas as; the design of radar absorbing materials, design of microwave and millimeter waveguides and components containing anisotropic materials (ferrites, plasma waveguides), design of composite perfect conductor-dielectric systems which exhibit backward propagation characteristics (periodically placed wires in a waveguide) [2], design of opto-electronic waveguides and devices and many other areas as well.

A useful mathematical technique [3, 4, 8] which greatly aids in the analysis of electromagnetic fields in anisotropic homogeneous materials consists of using a coordinate change of variables which when substituted in Maxwell's anisotropic equations, reduces Maxwell's equations to a Helmholtz wave equation, an equation for which well known solutions exist. Monzon [8] has used this technique to derive the Green's function of homogeneous, anisotropic materials located in unbounded space for the case when just three nonzero EM field components were excited. In a recent paper Jarem [3] introduced a modification of the coordinate transformation developed by Monzon [8] to derive the Green's function corresponding to a homogeneous anisotropic half space bounded by a Perfect Electric Conductor (PEC) or by a Perfect Magnetic Conductor (PMC). Fourier transform theory was used to derive the Green's function and in [3], several numerical examples of the Green's function were presented. The just described modified transformation of Jarem [3] has also been recently applied to study the resonant frequency of an anisotropic, inhomogeneous resonant cavity [4]. In this work, a resonant frequency analysis of a parallelogram cavity consisting of three PEC walls and one PMC wall was performed. The analysis was performed by solving the Helmholtz wave equation (expressed in x', y' coordinates [3]) for the EM fields in the cavity, forming a stationary variational expression for the resonant frequency of the cavity, and then finally, minimizing the variational expression using trial functions approximately meeting EM boundary conditions on the three PEC walls and the one PMC wall of the cavity.

The purpose of the present paper will be to further the study of propagation and calculation of EM fields in anisotropic waveguides by using the modified coordinate transformation of [3] to determine the EM fields that are associated with and that are excited in an

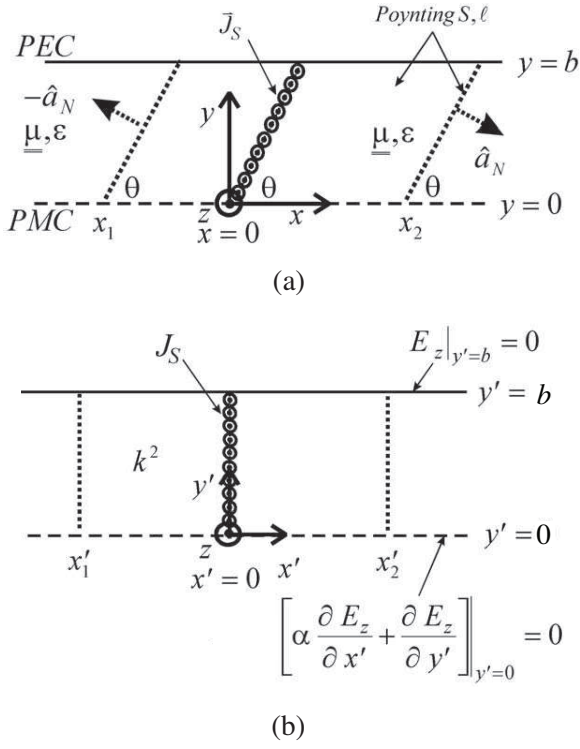

Figure 1. (a) The basic geometry of the anisotropic parallel plate waveguide system is shown, (b) including boundary conditions on the E_z electric field, is shown in dimensionless, transformed coordinates x', y'. The "*Poynting Box S*, ℓ" ($x_1' \leq x' \leq x_2'$) may or may not enclose the source.

anisotropic, parallel plate waveguide system. The specific parallel plate waveguide system to be studied is assumed to be infinite in extent, bounded by a perfect electric and a magnetic conductor wall (see Fig. 1), contain homogeneous, anisotropic material and is assumed to be excited by a novel electric slant-surface current (see Fig. 1). Advantages of using the modified coordinate transformation over using other mathematical techniques to study EM fields in anisotropic waveguides, is the fact that the coordinate transformation allows the easy solution and identification of the surfaces of constant phase possessed by the propagating modes of the system. These surfaces have the form $x' = (\sigma_P/\tau)x + \sigma_M y = cons\tan t$ (see Fig. 1) and knowledge of these surfaces are useful for indicating the direction

of real power flow of a given propagating mode, are useful for the study of modal orthogonality between different waveguide modes, and are useful for the design of efficient EM sources. The specific values of the numerical waveguide example were chosen so that one of the modes had the property that its phase velocity and direction of power flow were in opposite directions (backward wave). The source used to excite EM fields in the waveguide system has been chosen to be a novel electric, straight-line, slant surface current excitation (Fig. 1(a)) whose location coincided with the constant phase planes of the exponential factor corresponding to propagating mode solutions of the system. Very little constructive and destructive interference was observed between the modes excited by this source. The author believes that other mathematical techniques and methods that may be used to solve the mixed-partial differential equation resulting from Maxwell's anisotropic equations (See [3]) for the present problem, such as a direct solution by using a y-acting ordinary differential operator with constant coefficients, such as a finite difference or finite element method, or such as an integral equation technique cannot lead to as simple a solution for the EM fields and surfaces of constant phase of the propagating modes of the waveguide system as provided by the coordinate transformation method described herein.

A motivation of the paper is to use the anisotropic modal and source excitation analysis presented herein to calculate EM field and scattering as results when an anisotropic, inhomogeneous material-perfect conductor object is placed in an anisotropic waveguide [9]. The Rigorous Coupled Wave Analysis (RCWA) method [7, 10, 11] is an effective spectral domain method for determining the EM fields within an inhomogeneous, anisotropic material object. It consists of dividing the material object into a number of thin layers, using Floquet theory to solve Mawxell's equations in each thin layer, and then, using a boundary-condition matching ladder analysis, determining the overall form of the EM fields inside the material object. By summing the anisotropic, waveguide modes calculated in the present paper to determine the general form of the EM fields exterior to the scattering object and then boundary matching these EM fields to the internal EM fields found by the RCWA method, the overall EM fields of the whole system may be found. The orthogonality properties of the anisotropic waveguide modes established herein will be useful in implementing an accurate numerical analysis of the overall system equations for this problem.

As far as the author knows, this paper presents for the first time an anisotropic parallel plate waveguide analysis using the modified, anisotropic transformation coordinates which are defined by Jarem [3].

Several new results are presented in the paper including; a derivation of a novel characteristic equation to calculate backward propagation constants in the waveguide accurately; a novel study of backward and forward waveguide orthogonality and source excitation based on the complex Poynting theorem and an EM power reaction integral equation; and a study of the EM fields and power in an anisotropic parallel plate waveguide excited by a novel electric slant-line surface current source.

2. BASIC ANISOTROPIC WAVEGUIDE PROBLEM

The present analysis is concerned with determining the propagating and complex wave modes which can propagate in an anisotropic parallel plate waveguide which is bounded by a perfect electric conductor at $\widetilde{y} = \widetilde{y}' = \widetilde{b}$ (units of (meters)) and bounded by a perfect magnetic conductor at $\widetilde{y} = 0$ operating at an angular frequency ω: (1) when the nonzero EM field components have the form $E_z(\widetilde{x}, \widetilde{y}) \neq 0$, $H_x(\widetilde{x}, \widetilde{y}) \neq 0$, $H_y(\widetilde{x}, \widetilde{y}) \neq 0$; (2) when the magnetic permeability tensor of the system $\underline{\underline{\widetilde{\mu}_f}} = \widetilde{\mu}_f \underline{\underline{\mu}}$ has the following nonzero relative permeability components $\mu_{xx} = 4.4$, $\mu_{yy} = 1.1$, $\mu_{xy} = \mu_{yx}^* = 0.6 + j0.2116601$([3, 4]), $\mu_{zz} \neq 0$; and (3) when the permittivity of the system is isotropic and specified by $\widetilde{\varepsilon} = \widetilde{\varepsilon}_f \varepsilon$ ($\widetilde{\mu}_f, \widetilde{\varepsilon}_f$ are the permeability and permittivity values of free space, respectively). As shown in [3] with the substitution of $E_z(\widetilde{x}, \widetilde{y}) \neq 0$, $H_x(\widetilde{x}, \widetilde{y}) \neq 0$, $H_y(\widetilde{x}, \widetilde{y}) \neq 0$ in Maxwell's equation and introducing normalized coordinates defined by $x = \widetilde{k}_f \widetilde{x}$, $y = \widetilde{k}_f \widetilde{y}$ ($\widetilde{k}_f = 2\pi/\widetilde{\lambda}_f$, where $\widetilde{\lambda}_f$ is the free space wavelength in meters, $\omega = 2\pi f = \widetilde{k}_f c$ (rad/sec) is angular frequency, f is frequency in $(Hertz)$, and $c = 1/\sqrt{\widetilde{\mu}_f \widetilde{\varepsilon}_f}$ is the vacuum velocity of light) and using the transformation coordinates defined by Jarem [3]

$$x' = \frac{\sigma_P}{\tau} x + \sigma_M y, \; y' = y \tag{1}$$

it is found that Maxwell's equations reduce to the Helmholtz wave equation given by

$$\frac{\partial^2 E_z}{\partial x'^2} + \frac{\partial^2 E_z}{\partial y'^2} + k^2 E_z = 0 \tag{2}$$

where $k^2 = \varepsilon\gamma/\mu_{yy}$, $\gamma = \widetilde{\gamma}/\widetilde{\mu}_f^2 = [\widetilde{\mu}_{xx}\widetilde{\mu}_{yy} - \widetilde{\mu}_{xy}\widetilde{\mu}_{yx}]/\widetilde{\mu}_f^2 \neq 0$, $\tau = \sqrt{\widetilde{\mu}_{xx}/\widetilde{\mu}_{yy}}$, $\sigma_{1,2} = [2 \pm (\widetilde{\mu}_{xy} + \widetilde{\mu}_{yx})/\sqrt{\widetilde{\mu}_{xx}\widetilde{\mu}_{yy}}]^{1/2}$, $\sigma_P = 2/\sigma_1\sigma_2$ and $\sigma_M = (\sigma_2^2 - \sigma_1^2)/2\sigma_1\sigma_2$. Fig. 1(a) displays the geometry of

the waveguide system in x, y coordinates and Fig. 1(b) displays the geometry of the waveguide system in x', y' transformation coordinates. Using the x', y' coordinates (Eq. (1)) it is found that the magnetic field $\vec{H}$ is given by

$$\vec{H} = \frac{j\mu_{yy}}{\widetilde{\eta}_f \gamma} \left\{ \left(\alpha \frac{\partial E_z}{\partial x'} + \frac{\partial E_z}{\partial y'} \right) \hat{a}_x - \left(\beta_x \frac{\partial E_z}{\partial x'} + \beta_y \frac{\partial E_z}{\partial y'} \right) \hat{a}_y \right\} \qquad (3)$$

where $\alpha = \left(\frac{\mu_{xy}}{\mu_{yy}}\right)\left(\frac{\sigma_P}{\tau}\right) + \sigma_M$, $\beta_x = \sigma_P \tau + \left(\frac{\mu_{yx}}{\mu_{yy}}\right)\sigma_M$ and $\beta_y = \frac{\mu_{yx}}{\mu_{yy}}$.

The anisotropic parameters listed above have the values [3]: $\tau = 2.0$, $\gamma = 4.4352$, $\sigma_1 = 1.5954480$, $\sigma_2 = 1.206045$ (in [3], σ_2 was miss-listed as "*1.2066045*" with an incorrect "**6**" inserted as shown), $\sigma_P = 1.0394023$, $\sigma_M = -0.2834733$, $\alpha = 0 + j0.1$, $\beta_x = 1.92418277 + j0.05454545$ and $\beta_y = 0.54545454 - j0.19241827$. The angle θ shown in Fig. 1(a) is derived from the equation $x' = 0 = (\sigma_P/\tau)x + \sigma_M y$ (or $y = \tan(\theta)x$, $\tan(\theta) = \sigma_P/(-\sigma_M\tau) > 0$, as $0 < -\sigma_M$), and for the present anisotropic case, has the value $\theta = 61.3895403°$ The slant line equation just described in x, y coordinates shown in Fig. 1(a) represents the $x' = 0$ vertical line shown in Fig. 1(b). In [4] an example of a spatially inhomogeneous, magnetic anisotropic *PEC* waveguide whose symmetry properties resulted in a *PMC* boundary at $y = 0$ is presented and discussed.

3. MODAL CHARACTERISTIC EQUATION

This section is concerned with deriving the characteristic equation from which the wavenumbers of the propagating and complex modes associated with the anisotropic parallel plate waveguide in the waveguide (see Fig. 1) may be found. The EM fields of these modes, using the x', y' coordinates of Eq. (1) [3, Eq. (6c)] satisfy the Helmholtz wave equation (Eq. (2)), satisfy the EM boundary conditions that the E_z be zero at $y = y' = b$ ($b = \widetilde{k}_f \widetilde{b} = 1$ herein) and H_x be zero at $y = y' = 0$, and thus E_z satisfies the boundary condition

$$\left[\alpha \frac{\partial E_z}{\partial x'} + \frac{\partial E_z}{\partial y'} \right] \Bigg|_{y'=y=0} = 0 \qquad (4)$$

Solving the Helmholtz wave equation using separation of variables, satisfying the Dirichlet E_z boundary condition at $y = y' = b$ using $E_z = E_0 \exp(-k_x x') \sin(k_y(b - y'))$, and substituting this E_z in Eq. (4), it is found using $k_x^2 - k_y^2 + k^2 = 0$, $(j\alpha_I)k_x \sin(k_y b) + k_y \cos(k_y b) = 0$, where $\alpha_I = \mathrm{Im}ag(\alpha)$. Solving for $k_x = [k_y^2 - k^2]^{1/2}$, substituting, and

multiplying the resulting equation by b, it is further found

$$(j\alpha_I)\left[(k_yb)^2-(kb)^2\right]^{1/2}\sin(k_yb)+(k_yb)\cos(k_yb)=0 \tag{5}$$

For physically correct solutions in the region $x'\to\infty$ we require that $\mathrm{Re}al(k_x)=\mathrm{Re}al[k_y^2-k^2]^{1/2}\geq 0$ in order that E_z remain bounded. The total electric field which remains finite in a region where $x'\to\infty$, for a general value of the material wavenumber value $k=(\varepsilon\gamma/\mu_{yy})^{1/2}$ (Eq. (2)) after solving Eq. (5), consists of a sum of N_P propagating modes and an infinite sum of complex modes which attenuate exponentially as $x'\to\infty$, and is given by

$$E_z^+=\sum_{n=1}^{\infty}a_n^+\exp(-k_{xn}^+x')\sin(k_{yn}^+(b-y')) \tag{6}$$

where

$$k_{xn}^+\equiv k_{xn}=\begin{cases} jk_{xnI}, & n=1,\ldots,N_P \\ k_{xnR}+jk_{xnI}, & n=N_P+1,\ldots,\infty \end{cases} \tag{7a}$$

$$k_{yn}^+\equiv k_{yn}=\begin{cases} k_{ynR}, & n=1,\ldots,N_P \\ k_{ynR}+jk_{ynI}, & n=N_P+1,\ldots,\infty \end{cases} \tag{7b}$$

where k_{xnR}, k_{xnI}, k_{ynR}, k_{ynI} are real numbers, k_{yn} represents solutions of the characteristic equation Eq. (5), and $\mathrm{Re}al(k_{xn}^+)=\mathrm{Re}al(k_{xn})=\mathrm{Re}al[k_{yn}^2-k^2]^{1/2}\geq 0$. The general form of the electric field E_z, call it E_z^-, remaining finite in a region $x'\to-\infty$ may be found from the numerical solution for the wavenumbers k_{xn}^+, k_{yn}^+ given by Eqs. (7a), (7b) with a_n^-,k_{xn}^-,k_{yn}^- replacing a_n^+,k_{xn}^+,k_{yn}^+ respectively, and taking $k_{xn}^-=-k_{xn}^{+^*}$, $k_{yn}^-=k_{yn}^{+^*}$ in Eq. (6). We note overall that the propagating mode solutions for the $E_z^\pm$ field hold for the entire region $-\infty\leq x'\leq\infty$, and it's important to note that these modes may have real positive flow in either the positive or negative $\hat{a}_N$ directions (see Fig. 1(a)). When using $E_z^\pm$ to solve source excitation problems, one must keep only those modes radiating positive real power away from the source and attenuating to zero at $x=\pm\infty$.

Equation (5) represents a complex transcendental, characteristic equation for the propagating or complex mode wavenumber k_y of the system. In the limiting case when $\alpha_I\to 0$, the solutions for k_yb in Eq. (5) approach $k_mb=(m-0.5)\pi$, $m=1,2,3,\ldots$, and when α_I is small, but nonzero, the complex magnitude of k_yb, $|k_yb|$, is close to the value of k_mb, $m=1,2,3,\ldots$. In carrying out the solution of Eq. (5), two separate analyses need to be performed, one when k_yb is

not close to $k_m b$ and one when it is. In the first case a complex number, root-finding algorithm may be used to find the solutions for $k_y b$ and in the second case when $k_y b$ is very close to $k_m b$, it is useful to make a change of variables in the characteristic equation (Eq. (5)). Letting $k_x b = ju[2k_m b + 2\Delta - u^2]^{1/2}$, $k_y b = k_m b - u^2 + \Delta$, $\Delta = (k - k_m)b$, where $k = (\varepsilon\gamma/\mu_{yy})^{1/2}$, the characteristic equation (Eq. (5)), after algebra, may be expressed as

$$\begin{aligned} D_L(u,\Delta) &\equiv -\alpha_I[2k_m b + 2\Delta - u^2]^{1/2} u \\ &= [k_m b + \Delta - u^2]\left[\frac{-\tan(u^2) + \tan(\Delta)}{1 + \tan(u^2)\tan(\Delta)}\right] \equiv D_R(u,\Delta) \quad (8) \end{aligned}$$

Figure 2 for the value of $m = 3$ displays plots of the functions $D_L(u,\Delta)$ and $D_R(u,\Delta)$ of Eq. (8) over the interval $-0.02 \leq u \leq 0.08$, for values of the parameter Δ ranging from $\Delta = -10 \times 10^{-4}$, -6.5×10^{-4}, -5×10^{-4}, and $\Delta = 5 \times 10^{-4}$. The $D_R(u,\Delta)$ plot for the value of $\Delta = -5 \times 10^{-4}$, used for calculations in the paper, is the negative parabola, *solid* line plot which intersects the $D_L(u,\Delta)$ *solid* line plot at the points $u = u_1 = 0.014$ and $u = u_2 = 0.038$ (shown in Fig. 2). The resulting $k_x(u)$ wavenumbers for these u values turned out to be $k_x(u_1) = jk_{xI}(u_1) = j0.0536671$ (k_{x6I} in Table 1 is a backward mode) and $k_x(u_2) = jk_{xI}(u_2) = j0.146364$ (k_{x3I} in Table 1). Tables 1

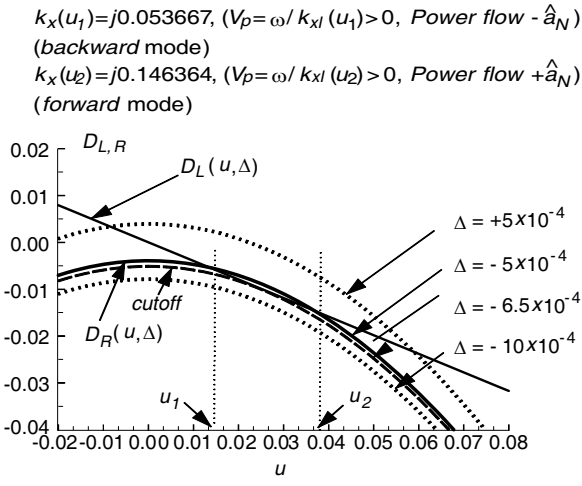

Figure 2. The left and right $D_L(u,\Delta)$, $D_R(u,\Delta)$ hand sides of the characteristic equation, Eq. (8) are plotted as a function of u ($\Delta = (k - k_m)b$).

and 2 list examples of the k_{xn}^{+}, k_{yn}^{+} and k_{xn}^{-}, k_{yn}^{-} modal wavenumbers that correspond to the numerical case described in Sec. 2.

4. COMPLEX POYNTING THEOREM AND REACTION POWER INTEGRAL EQUATION

Two important closely related mathematical equations derived from Maxwel's equations useful for establishing orthogonality properties of waveguide modes and for studying how EM sources excite waveguide modes in a parallel plate waveguide are the complex Poynting theorem integral equation and the reaction [12] power integral equation. The complex Poynting theorem integral equation when applied to the two dimensional parallel plate waveguide problem of the present problem is given by

$$P_f + j2\omega[W_M - W_E] = P_S \tag{9}$$

where $P_f = \oint_\ell \vec{S} \cdot \hat{a}_n d\widetilde{\ell}$, $W_M = \iint_S \mathcal{W}_M d\widetilde{A}$, $W_E = \iint_S \mathcal{W}_E d\widetilde{A}$, $P_S = \iint_S \mathcal{P}_S d\widetilde{A}$, and where $\vec{S} = \vec{E} \times \vec{H}^{\,*}/2$, $\mathcal{W}_M = \vec{B} \cdot \vec{H}^{\,*}/4$, $\mathcal{W}_E = \vec{D} \cdot \vec{E}^{\,*}/4$, $\mathcal{P}_S = -\vec{E} \cdot \vec{J}_V^{\,*}/2$, where S is the parallelogram Poynting box shown in Fig. 1(a). ($\widetilde{x}, \widetilde{y}$, etc. are unnormalized coordinates (units of meters)). The anisotropic parameters μ_{xx}, μ_{yy} are real and positive, the anisotropic parameters μ_{xy}, μ_{yx} are complex conjugates of one another, $\mu_{xy} = \mu_{yx}^{*} = \mu_R + j\mu_I$, thus

$$\begin{aligned} \mathcal{W}_M &= \frac{1}{4}\vec{B} \cdot \vec{H}^{\,*} = \frac{1}{4}[B_x H_x^{*} + B_y H_y^{*}] \\ &= \frac{1}{4}[\mu_{xx} H_x H_x^{*} + \mu_{xy} H_y H_x^{*} + \mu_{yx} H_x H_y^{*} + \mu_{yy} H_y H_y^{*}] \end{aligned} \tag{10}$$

thus $\mathcal{W}_M$ is real, as the terms $\mu_{xy} H_y H_x^{*}$ and $\mu_{yx} H_x H_y^{*}$ are complex conjugates of each other. The current source $\vec{J}_V$ is taken to be a limiting large amplitude, electric volume current source $\vec{J}_V = J_z(\widetilde{x}, \widetilde{y})\hat{a}_z$ (units Amps/m^2) distributed over a limiting small, parallelogram region. In the limit as the small parallelogram region approaches zero, the volume current acts like a surface current $\vec{J}_s(y) = J_S(y)\hat{a}_z$ distributed over the slant line $y = \tan(\theta)x$ (See Fig. 1(a)).

We will now evaluate the integrals of the complex Poynting Theorem as given by Eq. (9). When the Poynting box of Fig. 1 encloses the volume source $\vec{J}_V$ of Eq. (9) and is integrated over the region where

$\vec{J}_V$ is nonzero, the P_S integral of Eq. (9) is given by

$$P_{JS} = -\frac{1}{2\widetilde{k}_f \sin(\theta)} \int_0^b E_z(0, y') J_S^*(y') dy' \tag{11}$$

where E_z is expressed in x', y' coordinates with $x' = 0$. We will now evaluate $P_f = \oint_\ell \vec{E} \times \vec{H}^* /2 \cdot \hat{a}_n d\widetilde{\ell}$ over the Poynting box. On the upper $\widetilde{y} = \widetilde{b}$ edge, the integrand is zero because $\vec{E}_{\widetilde{y}=\widetilde{b}} = E_z|_{\widetilde{y}=\widetilde{b}} \hat{a}_z = 0$, and thus the integral over this edge is zero. On the lower edge ($\widetilde{y} = 0$) the integrand of P_f the integral, namely, $\vec{E} \times \vec{H}^* \cdot \hat{a}_n|_{\widetilde{y}=0} = \vec{E} \times \vec{H}^* | \cdot (-\hat{a}_y)|_{\widetilde{y}=0} = -E_z H_x^*|_{\widetilde{y}=0} = 0$ because $H_x|_{\widetilde{y}=0} = 0$ and thus the integral over this edge is zero. On the right most slant edge of the box of Fig. 1(a) the P_f integrand is $\vec{E} \times \vec{H}^* \cdot \hat{a}_N = E_z \hat{a}_z \times (H_T^* \hat{a}_T + H_N^* \hat{a}_N) \cdot \hat{a}_N = -E_z H_T^*$, $\hat{a}_T = \cos(\theta)\hat{a}_x + \sin(\theta)\hat{a}_y$, $\hat{a}_N = \sin(\theta)\hat{a}_x - \cos(\theta)\hat{a}_y$, where $H_T = \cos(\theta)H_x + \sin(\theta)H_y$. H_T represents the magnetic field component tangential (or parallel) to the right most slant edge of the Poynting box and H_N is the normal component. It is useful to express H_T in terms of dimensionless transformation coordinates x', y'. The quantity H_T may be expressed in transformation coordinates as

$$H_T = \frac{j}{\widetilde{\eta}_f} \frac{\mu_{yy}}{\gamma} \left[t_x \frac{\partial E_z}{\partial x'} + t_y \frac{\partial E_z}{\partial y'} \right] \tag{12}$$

where t_x, t_y are coefficients given by

$$t_x \equiv t_{xR} = \alpha \cos(\theta) - \beta_x \sin(\theta) = -\left[\sigma_P \tau + \frac{\mu_R}{\mu_{yy}} \sigma_M \right] \sin(\theta) \tag{13a}$$

$$t_y \equiv j t_{yI} = \cos(\theta) - \beta_y \sin(\theta) = j \frac{\mu_I}{\mu_{yy}} \sin(\theta) \tag{13b}$$

where $\mu_R = \mathrm{Re}al(\mu_{xy})$, $\mu_I = \mathrm{Im}ag(\mu_{xy})$. For the anisotropic numerical case specified in Sec. 2, $t_{xR} = -1.6892315367$ and $t_{yI} = 0.16892315367$. When H_T of Eq. (12) is substituted in P_f of Eq. (9), and integrated along the right most slant edge of the Poynting box (lowest part of edge located at $x = x_2$ (see Fig. 1(a)), this edge corresponds $x' = x_2'$ of Fig. 1(b)) using the y' coordinate as an integration variable (note that $d\ell = dy'/\sin(\theta)$, $dy = dy'$), it is found the P_f integral on this edge,

call it P_{f2}, has a value

$$P_{fe} = \frac{-1}{2\widetilde{k}_f \sin(\theta)} \int_0^b E_z H_T^* dy' = j\widetilde{S}_f \int_0^b E_z \left[t_x \frac{\partial E_z}{\partial x'} + t_y \frac{\partial E_z}{\partial y'} \right]^* \Big|_{x'=x'_e} dy' \quad (14)$$

$$\widetilde{S}_f = \frac{\mu_{yy}}{2\widetilde{k}_f \widetilde{\eta}_f \gamma \sin(\theta)} \quad (15)$$

where $P_{f2} = P_{fe}$ when $x'_e = x'_2$. At the leftmost slant edge of the Poynting box of Fig. 1(a), the P_f integral on this edge, call it the P_{f1}, is given by the P_{fe} integral of Eq. (14) with x'_e set equal to x'_1 and the sign of the integral reversed, because the outward normal on the leftmost face is $-\hat{a}_N$, opposite to that of the rightmost face which is $\hat{a}_N$ (see Fig. 1(a)). Eq. (14) can be used to evaluate all power slant angle integrals as long as the correct sign of the outward normal (left or right) is accounted for in the final integrated power expressions.

The reaction power integral equation is derived from Maxwell's equations and application of the divergence theorem, and is given by

$$P_{Rf} = j2\omega[-W_{RM} - W_{RE}] + P_{RS} \quad (16)$$

where $P_{Rf} = \frac{1}{2} \oint_\ell \vec{E} \times \vec{H} \cdot \hat{a}_n d\widetilde{\ell}$, $W_{RM} = \frac{1}{4} \iint_S \vec{B} \cdot \vec{H} d\widetilde{A}$, $W_{RE} = \frac{1}{4} \iint_S \vec{D} \cdot \vec{E} d\widetilde{A}$, $P_{RS} = -\iint_S (\vec{E} \cdot \vec{J}_V/2) d\widetilde{A}$. As $\vec{H}$ and $\vec{H}^*$ satisfy the same boundary conditions, and as the integral is taken over the same parallelogram area S (Poynting box of Fig. 1(a)) as Eq. (9), we find, following the same steps as were used to evaluate P_f of Eq. (14), that $P_{Rf} = P_{Rf2} + P_{Rf1}$ where

$$P_{Rfe} = -j\widetilde{S}_f \int_0^b E_z \left[t_x \frac{\partial E_z}{\partial x'} + t_y \frac{\partial E_z}{\partial y'} \right] \Big|_{x'=x'_e} dy' \quad (17)$$

where P_{Rf2} is given by P_{Rfe} of Eq. (17) with x'_e set equal to x'_2, and P_{Rf1} is given by P_{Rfe} of Eq. (17) with x'_e set equal to x'_1 and the sign of the integral reversed to account for the outward normal $\hat{a}_n = -\hat{a}_N$ being opposite to that used for P_{Rf2} (see Fig. 1(a)). The volume current source of integral namely P_{RS} of Eq. (16) is evaluated in the same way as P_{JS} of Eq. (11) except that one uses $\vec{J}_V$ to evaluate P_{RS} rather than $\vec{J}_V^*$ as was used to evaluate Eq. (11). The reaction power integral equation is very useful for determining the excitation of waveguide modes when an electric current source is present.

The complex Poynting theorem equation is useful for studying waveguide mode orthogonality as will be shown by the following analysis. First when a linear combination of waveguide modes (having

the separated form $X_n(x')Y_n(y')$, Sec. 3), whose orthogonality is to be studied, are assumed to be excited in a parallelogram Poynting box (see Fig. 1(a)), and the power flow integral P_f of Eq. (9) is evaluated, it turns out that that the only nonzero contribution to this integral occurs across the slant edges of the Poynting box (Eq. (14)). Secondly, if the Poynting box is assumed to be source free, this further means that in the complex Poynting theorem equation, the P_S term of Eq. (9) is zero. Thus Eq. (9) reduces to $P_{f1} + P_{f2} + j2\omega[W_M - W_E] = P_S = 0$, where P_{f1}, P_{f2}, are the slant edge integrals of Eq. (14). Taking the real part of this equation, using the fact that real part of the energy difference term of this equation is zero, (due to the fact that $j2\omega[W_M - W_E]$ is purely imaginary as W_M, W_E are purely real), we find $\mathrm{Re}al(P_{f1} + P_{f2}) = 0$. When the linear combination of waveguide modes to be studied is now substituted in P_{f1}, P_{f2} of this equation, the $\vec{E}\times\vec{H}^{\,*}/2$ cross product and the slant edge integrations are evaluated, one notes then that in each n, n' cross product term, that the factor $X_n(x')X^*_{n'}(x')$, $x' = x'_1, x'_2$ (x'_1, x'_2 represent the location of the slant edges of P_{f1}, P_{f2}, see Fig. 1(b)) is a constant. Thus it turns out that the quantities P_{f1}, P_{f2}, are each a n, n' double summation of the $X_n(x'_i)X^*_{n'}(x'_i)$, $i = 1, 2$ constant factor *times* a y'-integral, call it $I^{0:b}_{n,n'}(Y_n(y'), Y^*_{n'}(y'))$, $0 \le y' \le b$, of the $Y_n(y')Y^*_{n'}(y')$, $Y_n(y')dY^*_{n'}(y')/dy'$ products making up the $\vec{E} \times \vec{H}^{\,*}/2$ cross product. Since $\mathrm{Re}al(P_{f1} + P_{f2}) = 0$ must be zero for all values of x'_1, x'_2 over a very large range of continuous values of x'_1 and x'_2, the only way $\mathrm{Re}al(P_{f1} + P_{f2}) = 0$ can be zero then, is if appropriate combinations of the values of the real and imaginary parts of the $I^{0:b}_{n,n'}$ integrals are set to zero. The appropriate combinations of the values of the real and imaginary parts of the $I^{0:b}_{n,n'}$ integrals which are zero to make the $\mathrm{Re}al(P_{f1} + P_{f2}) = 0$, then represent the orthogonality relations that are satisfied by the waveguide modes of the system. We mention now that once these relations have been established, they may be used to derive additional waveguide orthogonality relations based on the reaction power integral $P_{Rf} = \oint_\ell \vec{E} \times \vec{H}/2 \cdot \hat{a}_n d\tilde{\ell}$.

The most important orthogonality relations that may be derived form the preceding discussion may be summarized as follows. When $n \neq n'$ we have the $\vec{E} \times \vec{H}^{\,*}/2$ power orthogonality condition that is given by

$$T^{-+}_{Pn'n} + T^{+-*}_{Pnn'} = 0 \tag{18}$$

where

$$T^{+-}_{Pnn'} = -jt_{xR}k^{-*}_{xn'}I_{S^+_n S^{-*}_{n'}} - t_{yI}k^{-*}_{yn'}I_{S^+_n C^{-*}_{n'}} \tag{19a}$$

$$T^{-+}_{Pn'n} = -jt_{xR}k^{+*}_{xn}I_{S^-_{n'} S^{+*}_n} - t_{yI}k^{+*}_{yn}I_{S^-_{n'} C^{+*}_n} \tag{19b}$$

$$I_{S^+_n S^{-*}_{n'}} = \int_0^b \sin k^+_{yn}(b-y')\sin k^{-*}_{yn'}(b-y')dy' \tag{20a}$$

$$I_{S^+_n C^{-*}_{n'}} = \int_0^b \sin k^+_{yn}(b-y')\cos k^{-*}_{yn'}(b-y')dy' \tag{20b}$$

and where $I_{S^-_{n'} S^{+*}_n}$, $I_{S^-_{n'} C^{+*}_{n'}}$ may be found from Eqs. (20a), (20b) by interchanging k^+_{yn} and $k^-_{yn'}$. When the E^+_z, E^-_z electric field linear combinations of Eqs. (6), (7) are substituted in the P_{Rfe} reaction integral of Eq. (17), it is found that the total power reaction of these fields is given by

$$P^{\pm}_{Rfe} = \widetilde{S}_f \sum_{n,n'} a^{\pm}_n a^{\pm}_{n'} X^{\pm}_n(x'_e) X^{\pm}_{n'}(x'_e) T^{\pm\pm}_{Rnn'} \tag{21}$$

where the *reaction power* coefficients $T^{++}_{Rnn'}$, $T^{--}_{Rnn'}$ in these equations are given by

$$T^{++}_{Rnn'} = jt_{xR}k^+_{xn'}I_{S^+_n S^+_{n'}} - t_{yI}k^+_{yn'}I_{S^+_n C^+_{n'}} = T^{+-}_{Pnn'} \tag{22a}$$

$$T^{--}_{Rnn'} = jt_{xR}k^-_{xn'}I_{S^-_n S^-_{n'}} - t_{yI}k^-_{yn'}I_{S^-_n C^-_{n'}} = T^{-+}_{Pnn'} \tag{22b}$$

where

$$I_{S^\pm_n S^\pm_{n'}} = \int_0^b \sin k^\pm_{yn}(b-y')\sin k^\pm_{yn'}(b-y')dy' \tag{23a}$$

$$I_{S^\pm_n C^\pm_{n'}} = \int_0^b \sin k^\pm_{yn}(b-y')\cos k^\pm_{yn'}(b-y')dy' \tag{23b}$$

and where the wavenumbers are defined in Sec. 3. Using the $\vec{E}\times\vec{H}^*/2$ power orthogonality relation, $T^{-+}_{Pn'n} + T^{+-*}_{Pnn'} = 0$, $n \neq n'$ (Eq. (18)), substituting $k^-_{xn} = -k^{+*}_{xn}$, $k^-_{yn} = k^{+*}_{yn}$ (Eqs. (6), (7)), it is found after algebra that the reaction the *reaction power* coefficients $T^{++}_{Rnn'}$, $T^{--}_{Rnn'}$, satisfy the following reaction power orthogonality equations, $n \neq n'$,

$$T^{++}_{Rnn'} + T^{++}_{Rn'n} = 0 \tag{24a}$$

$$T^{--}_{Rnn'} + T^{--}_{Rn'n} = 0 \tag{24b}$$

These equations, as mentioned earlier, are useful for defining a matrix equation from which to determine EM source excitation. The "*Plus, Minus*" superscript on the coefficient $T^{+-}_{Pnn'}$ in Eq. (19a), for example, indicates that n the waveguide mode is finite at $x' \to \infty$ and that the n' waveguide is finite at $x' \to -\infty$. Other '*Plus/Minus*" superscript combinations on the coefficients $T^{-+}_{Pn'n}$, $T^{++}_{Rnn'}$, $T^{--}_{Rnn'}$ refer to regions where the waveguide modes making up these coefficients remain finite at $x' \to \pm\infty$. It may be further shown that no real power is carried by complex modes or interactions with complex modes.

We now consider the special case when n and n' are both propagating modes. In this case we find, after substituting $k^+_{xn} = k^-_{xn} = jk_{xnI}$, $k^+_{yn} = k^-_{yn} = k_{ynR}$ (Eqs. (6), (7)) in Eqs. (18)–(24), that the sets of power and reaction coefficients in these equations are all real and are equal to one another for the same values n and n'. Thus letting this value be $T^{prop}_{nn'}$, we have $T^{prop}_{nn'} = T^{+-}_{Rnn'} = T^{-+}_{Rnn'} = T^{++}_{Rnn'} = T^{--}_{Rnn'}$, $(n, n') = 1, \ldots, N_P$. Thus substituting $T^{prop}_{nn'}$ in Eqs. (18)–(24), we find that the propagating modes satisfy the following orthogonality relation namely

$$T^{prop}_{nn'} + T^{prop}_{n'n} = 0 \tag{25}$$

where

$$T^{prop}_{nn'} = -t_{xR} k_{xn'I} I_{S_n S_{n'}} - t_{yI} k_{yn'R} I_{S_n C_{n'}} \tag{26}$$

$$I_{S_n S_{n'}} = \int_0^b \sin k_{ynR}(b - y') \sin k_{yn'R}(b - y') dy' \tag{27a}$$

$$I_{S_n C_{n'}} = \int_0^b \sin k_{ynR}(b - y') \cos k_{yn'R}(b - y') dy' \tag{27b}$$

and where $n \neq n'$. The T^{prop}_{nn} coefficient is useful for determining the $\vec{E} \times \vec{H}^*/2$ power associated with a propagating mode whose complex amplitude is a_n. The power associated with this mode in this paper will be defined to be that power which is transmitted through the slanted right edge of the Poynting box shown in Fig. 1 and is given by Eq. (14). The power of this mode is real, and due to the orthogonality relations derived earlier does not interact with the other propagating modes. It is given by

$$\widetilde{P}_n = \widetilde{S}_f |a_n|^2 T^{prop}_{nn} \tag{28}$$

where $\widetilde{S}_f$, T^{prop}_{nn} are defined by Eqs. (15), (26) respectively with $n = n'$. With the definition of power given in Eq. (28), if T^{prop}_{nn} is greater than zero ($T^{prop}_{nn} > 0$) this indicates that the integrated, positive power flow $|\widetilde{P}_n|$ of the mode is in the $+\hat{a}_N$ direction and if T^{prop}_{nn} is negative,

$T_{nn}^{prop} < 0$ this indicates that the integrated, positive power flow of the mode $|\widetilde{P}_n|$ is in the $-\hat{a}_N$ direction (see Fig. 1(a)). The sign of the power flow determined by T_{nn}^{prop}, is important when studying the excitation of a waveguide system, as it gives information about which modes transmit power away from the source, and therefore which modes should be physically included in the EM field solution of this problem. By selecting modes meeting proper EM boundary conditions at $x \to \pm\infty$, matching EM boundary conditions adjacent to the electric current source, and using the reaction orthogonality relations of Eqs. (24a), (24b) an efficient and accurate matrix equation to determine all modal excitation amplitudes of the system may be found. Using the proper expansion of anisotropic waveguide modes (20 modes), the source excitation matrix may also be derived by evaluating the reaction integral equation (Eq. (16)) over a vanishing small, Poynting box enclosing the electric current source $\vec{J}_s(y) = J_S(y)\hat{a}_z$ (W_{RM}, W_{RE} in Eq. (16) integrate to zero over this Poynting box).

5. NUMERICAL RESULTS

In this section numerical examples of the wavenumbers, modal interaction coefficients and demonstration of orthogonality of waveguide modes corresponding to the anisotropic parameter case described in Sec. 2 are presented, along with plots of the EM fields which result when the anisotropic waveguide displayed in Fig. 1 is excited by a surface current (Fig. 1). Further, to give a sense of how the anisotropy of the waveguide medium influences the EM fields in the waveguide, also presented in this section are the EM fields which are excited in a comparison isotropic waveguide when; (1) the frequency of operation, (2) the dimensions, (3) the exciting source, and (4) the boundary conditions, are all identical to that of the anisotropic waveguide. In addition, the material wavenumber of the isotropic waveguide, $k_{iso} = (\mu_{iso}\varepsilon_{iso})^{1/2}$, has been chosen to be very close, but just slightly higher in value, than the material wavenumber of the anisotropic waveguide, namely $k = (\varepsilon\gamma/\mu_{yy})^{1/2}$. Standard Green's function theory (300 modes) has been used to determine the EM fields of the isotropic comparison waveguide.

To study anisotropic, modal orthogonality and waveguide source excitation, the normalized wavenumber of operation $k = (\varepsilon\gamma/\mu_{yy})^{1/2}$ (assumed excited at the angular frequency $\omega = 2\pi f$ (rad/sec) of operation by $\omega = \widetilde{k}_f c$ (rad/sec), $\widetilde{k}_f = 2\pi/\widetilde{\lambda}_f$, $c = 1/\sqrt{\widetilde{\mu}_f\widetilde{\varepsilon}_f}$, velocity of light) of the anisotropic waveguide has been chosen so that $k = (\varepsilon\gamma/\mu_{yy})^{1/2} = \frac{\pi}{b}(m - 0.5) + \Delta = 7.85348163347$ where $m = 3$,

$\Delta = -5 \times 10^{-4}$ and $b = \widetilde{k}_f \widetilde{b} = 1$. For this chosen value of k and of the anisotropic parameters specified in Sec. 2, $\varepsilon = 15.2969180970$. Using this value of k, thirteen modes have been calculated in the region $x' \to \infty$ and thirteen modes in the source free region $x' \to -\infty$. Of these thirteen modes calculated in each region, six of them are propagating and the other seven are complex (or non propagating). In the region $x' \to \infty$, three of the propagating modes have real power flow in the $+\hat{a}_N$ direction (they are labeled $k_{xn}^{+} = jk_{xnI}$, $n = 1, 2, 3$), three of these modes have real power in the $-\hat{a}_N$ direction (they are labeled $k_{xn}^{+} = jk_{xnI}$, $n = 4, 5, 6$), and the other seven are complex modes and attenuate to zero as $x' \to \infty$ ($\exp(-k_{xn}^{+}x') \to 0, x' \to \infty$) (they are labeled $k_{xn}^{+} = k_{xnR} + jk_{xnI}$, $n = 7, \ldots, 13$, (Eq. (7a) gives k_{xn}^{+}). In the region $x' \to -\infty$, the propagating modes are identical to those in the region $x' \to \infty$ (they are labeled $k_{xn}^{-} = jk_{xnI}$, $n = 1, \ldots, 6$) and the other seven modes in this region are complex and attenuate to zero as $x' \to -\infty$ ($\exp(-k_{xn}^{-}x') \to 0, x' \to -\infty$) (they are labeled $k_{xn}^{-} = -k_{xnR} + jk_{xnI}$, $n = 7, \ldots, 13$). The mode labeling system just described has been chosen so that the interaction of forward and backward modes could be studied in a complete way. The wavenumber k_{iso} of the comparison isotropic waveguide has been taken to have a value of $k_{iso} = \frac{\pi}{b}(m - 0.5) + |\Delta| = 7.85448163347$, which is slightly higher than that used for the anisotropic waveguide. A slightly higher value of k_{iso} was chosen to ensure that both the isotropic and anisotropic waveguides had the same number of six propagating modes, and thus a meaningful comparison of results of the two systems could be made. The isotropic comparison waveguide relative dielectric permittivity and magnetic permeability was taken to be respectively $\varepsilon_{iso} = (k_{iso}^2 \mu_{yy})/\gamma = 15.3008139$ and $\mu_{iso} = k_{iso}^2/\varepsilon_{iso} = 4.0320000000$. Taking the normalized, waveguide height for both the anisotropic and isotopic cases to have a value of $b = \widetilde{b}\widetilde{k}_f = 1$, and taking, as an example, the unnormalized waveguide height have a value of $\widetilde{b} = 1.0\,(\mathrm{cm})$, we find that both waveguide systems are operating at a frequency of $f = c/\widetilde{\lambda}_f$, $\widetilde{\lambda}_f = 2\pi/\widetilde{k}_f = 2\pi\widetilde{b}$, or $f = c/(2\pi\widetilde{b}) = 4.774648\,\mathrm{GHz}$. The specific electric surface current source (Eq. (11)) that was chosen to excite EM fields in the anisotropic and comparison isotropic waveguides is defined (see the slant line of Fig. 1(a), $x = \cot(\theta)y$) by the equation

$$E_{JS}(y) \equiv \widetilde{\eta}_f J_S(y) = \widetilde{\eta}_f J_S(y') = \widetilde{\eta}_f J_{S0} \sin(k_{JS}(b - y))\ (\mathrm{V/m}) \quad (29)$$

where $y' = y$ (Eq. (1)), $b = \widetilde{k}_f \widetilde{b} = 1$, $\theta = 61.38954°$, $\widetilde{\eta}_f = 377\,\Omega$, $\widetilde{\eta}_f J_{S0} = 1.0\,(\mathrm{V/m})$, $k_{JS} = 0.7(\pi/b)(m - 0.5) = 5.497787$, $m = 3$.

Tables 1 and 2 list several values of propagation constants k_{xn}, k_{yn}, the $T_{nn'}^{prop}$, $T_{Pnn'}^{\pm\pm}$, $T_{Rnn'}^{\pm\pm}$ complex and reaction power coefficients, their

power flow characteristics and their on and off-diagonal orthogonality relations. Rows 1 and 2, Table 1 display normalized modal power P_3, P_6 of the $n = 3$, $n = 6$ anisotropic waveguide modes respectively (P_3, P_6 are normalized by $|P_{JS}^{ANI}|$ the magnitude of complex power delivered by slant source of Eq. (29)). The unnormalized power deliver by the source in the anisotropic waveguide when $\tilde{b} = 1.0\,\text{cm}$ (or $f = c/(2\pi\tilde{b}) = 4.774648\,\text{GHz}$) in the anisotropic waveguide was $P_{JS}^{ANI} = 1.3381118 \times 10^{-5} + j1.0684890 \times 10^{-8}$ (Watts/m) and in the

Table 1. On-diagonal power coefficients.

$T_{3,3}^{prop} = T_{R3,3}^{++} = T_{R3,3}^{--} = 3.913151 \times 10^{-2}$ $k_{x3}^{\pm} = jk_{x3I} = j0.146364, k_{y3}^{\pm} = k_{y3R} = 7.852117$ *Phase velocity* $(+\hat{a}_N)$, $v_{phase} \propto (\omega/k_{x3I}) > 0$ $P_3 = 0.4473 > 0$, *power flow* $+\hat{a}_N$ $P_3 = \widetilde{S}_f \lvert a_3\rvert^2 T_{3,3}^{prop}/\lvert P_{JS}^{ANI}\rvert$ (*Normalized Power*) (Forward)
$T_{6,6}^{prop} = T_{R6,6}^{++} = T_{R6,6}^{--} = -3.913736 \times 10^{-2}$ $k_{x6}^{\pm} = jk_{x6I} = j0.0536671, k_{y6}^{\pm} = 7.853298$ *Phase velocity* $(+\hat{a}_N)$, $v_{phase} \propto (\omega/k_{x6I}) > 0$ $P_6 = -0.4452 < 0$, *power flow* $-\hat{a}_N$ $P_6 = \widetilde{S}_f \lvert a_6\rvert^2 T_{6,6}^{prop}/\lvert P_{JS}^{ANI}\rvert$ (*Normalized Power*) (Backward)

Table 2. Off-diagonal orthogonality results.

$T_{1,6}^{prop} = -0.103492$, $T_{6,1}^{prop} = 0.103492$ $T_{1,6}^{prop} + T_{6,1}^{prop} = 2.82 \times 10^{-12}$
$T_{3,6}^{prop} = -0.0387554$, $T_{6,3}^{prop} = 0.0387554$ $T_{3,6}^{prop} + T_{6,3}^{prop} = -1.06 \times 10^{-13}$
$T_{2,3}^{prop} = 0.398420$, $T_{3,2}^{prop} = -0.398420$ $T_{2,3}^{prop} + T_{3,2}^{prop} = -3.32 \times 10^{-10}$
$T_{P6,8}^{+-} = T_{R6,8}^{++} = 6.01 \times 10^{-2} - j9.92 \times 10^{-4}$ $T_{P8,6}^{+-} = T_{R8,6}^{++} = -6.01 \times 10^{-2} + j9.92 \times 10^{-4}$ $T_{R6,8}^{++} + T_{R8,6}^{++} = 6.02 \times 10^{-12} + j1.81 \times 10^{-9}$ $k_{x8}^{\pm} = \pm 11.754964 + j0.100232$ $k_{y8}^{\pm} = 14.136946 \pm j0.083344$

isotropic waveguide was $P_{JS}^{ISO} = 1.3382489 \times 10^{-5} + j3.8284423 \times 10^{-8}$ (Watts/m). Also shown in Table 1 are the signs of the phase velocities of the modes. As can be seen from Table 1, the $n = 3$ waveguide mode corresponds to a forward mode as the phase velocity and power flow of this mode have the same sign, whereas the $n = 6$ waveguide mode corresponds to a backward mode as phase velocity and power for the $n = 6$ mode have opposite signs. Rows 1, 2, 3, and 4 of Table 2 display examples of the off-diagonal orthogonality relations that the anisotropic waveguide modes satisfy. As can be seen from these rows, the orthogonality relations are satisfied to a high degree of numerical accuracy. Its interesting to note in Row 2, Table 2, that the $n = 3$, forward mode, and the $n = 6$, backward mode (which together, as seen from Rows 1 and 2, Table 1 radiate about ninety percent of the power away from the electric current source) satisfy the orthogonality relation of Eq. (25) to a very high degree of accuracy.

Figure 3 shows, respectively, the real and imaginary part of the $E_z^+(y)$ and $E_z^-(y)$. for both the anisotropic and isotropic waveguide cases. The quantity $E_z^{\pm}(y)$ represents values of the parallel component of the electric field evaluated at points just to the right and left of the electric surface current source and these fields meet EM boundary conditions to a high degree of accuracy. Fig. 4 shows plots of $\mathrm{Im}ag(\widetilde{\eta}_f H_T^+(y))$ and $\mathrm{Im}ag(\widetilde{\eta}_f H_T^-(y))$ versus coordinate y for the isotropic (top) and anisotropic waveguide cases (bottom). Because $J_S(y)$ is purely real, the $\mathrm{Im}ag(H_T^+(y))$ should equal the $\mathrm{Im}ag(H_T^-(y))$ to a high degree of accuracy to meet the electric current-magnetic field boundary condition, and this is observed in the figures. An interesting feature of the $\mathrm{Im}ag(\widetilde{\eta}_f H_T^{\pm}(y))$ plots of the isotropic waveguide case, when compared to the $\mathrm{Im}ag(\widetilde{\eta}_f H_T^{\pm}(y))$ plots of the anisotropic waveguide case, is the fact that the absolute value of the imaginary part of the tangential magnetic field ($\mathrm{Im}ag(H_T^{\pm}(y))$) for the isotropic case is much larger and has a much smoother and different shape than does the corresponding tangential magnetic field ($\mathrm{Im}ag(H_T^{\pm}(y))$) for the anisotropic case. The smallness of the imaginary part of the magnetic field in the anisotropic case relative to the isotropic one is probably due to the fact that in the anisotropic case the source is located on a phase plane where all the modes have the same phase. Fig. 5(a) and 5(b) show plots $\mathrm{Re}al(E_z(x, y))$ for the anisotropic and isotropic waveguide cases, respectively. In comparing the anisotropic and isotropic plots for the $\mathrm{Re}al(E_z(x, y))$ and field components, it is clearly noticed that $\mathrm{Re}al(E_z(x, y))$ in the region $-240 < x < 0$ of the anisotropic plots (Fig. 5(a)) has a far different wave structure and shape than the $\mathrm{Re}al(E_z(x, y))$ in the region $0 < x < 240$, whereas the electric field components plots

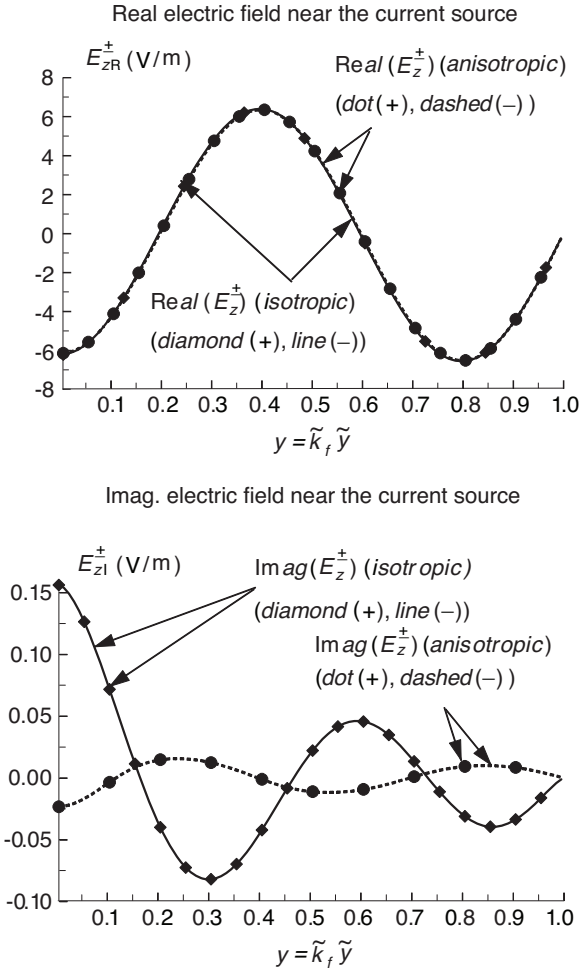

Figure 3. Plots of tangential electric field components, just to the right and left slanted surface current $J_S(y)$.

corresponding to the isotropic waveguide case (Fig. 5(b)) has the nearly the same wave structure in the all regions of the plots $-240 < x < 240$. The difference in the Re$al(E_z(x, y))$ waveshape for the anisotropic case in the regions $-240 < x < 0$ and $0 < x < 240$, is due the anisotropy of the medium causing different interference patterns in the two regions. The positive and negatively propagating modes in the isotropic waveguide case have the same waveguide wavelength, and thus they have the same wave structure in the region $-240 < x < 240$.

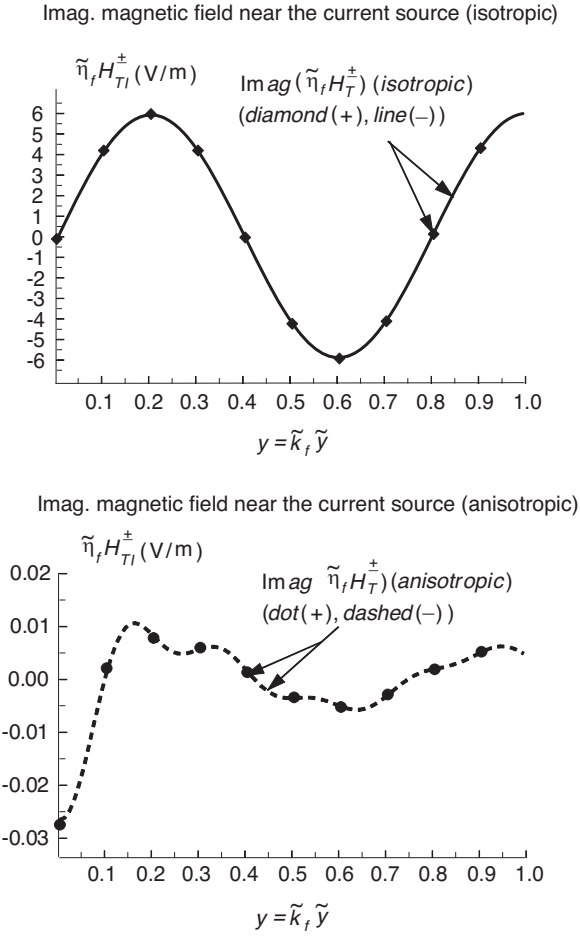

Figure 4. Plots of Im$ag(\widetilde{\eta}_f H_T^+)$, Im$ag(\widetilde{\eta}_f H_T^-)$, $\widetilde{\eta}_f = 377\,\Omega$ just to the right and left slanted surface current $J_S(y)$.

In Figs. 5(a), 5(b) the boundary condition Re$al(E_z(x, y)) = 0$ is seen to hold at $y = b = 1$.

For numerical calculations made for the anisotropic and isotropic waveguide cases studied it was found that EM boundary conditions near the surface current and near the waveguide walls were satisfied to a high degree of accuracy and that power conservation held to a high degree of accuracy. Specifically, defining conservation of *complex power* error for the anisotropic waveguide case, call it E_P^{ANI}, as the difference between normalized integrated complex $\vec{E} \times \vec{H}^*/2$ power

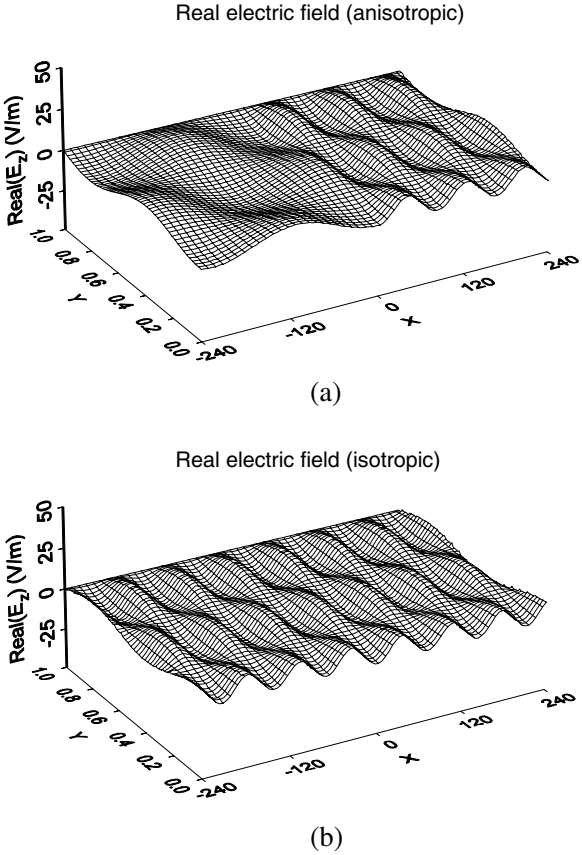

Figure 5. Plots of the Re$al(E_z(x, y))$, for the (a) anisotropic case and (b) isotopic case.

radiated from the source and delivered by the source, it was found $E_P^{ANI} = 1.405 \times 10^{-4} + j6.404 \times 10^{-4}(\%)$. Defining conservation of *reaction power* error, call it E_P^{ANI}, as the difference between normalized *reaction* $\vec{E} \times \vec{H}/2$ *power* radiated from the source and delivered by the source, it was found $E_R^{ANI} = 4.095 \times 10^{-8} + j1.651 \times 10^{-10}(\%)$. As seen from the just listed error values, conservation of *complex* and *reaction power* are both obeyed to a high degree of accuracy, with *reaction power* error being much smaller than *complex power* error. Conservation of real normalized power for the isotropic waveguide case was also calculated and found to hold to an accuracy of about $0.01(\%)$.

6. SUMMARY AND CONCLUSIONS

The excitation of backward and forward, EM modes and fields in an anisotropic, parallel plate waveguide (meeting Dirichlet and Neumann boundary conditions) has been studied using a modified coordinate transformation [3, 4] which reduces the Maxwell's equations of the system to the form of a Helmholtz wave equation satisfying Dirichlet and mixed-partial derivative boundary conditions. Overall the modal, orthogonality, and source analysis carried out herein should be useful for the calculation anisotropic waveguide Green's functions and the associated study of EM scattering as results when different metal or material objects are placed in an anisotropic waveguide.

REFERENCES

1. Rodriguez-Berral, R., F. Mesa, and F. Medina, "Appropriate formulation of the characteristic equation for open nonreciprocal layered waveguides with different upper and lower half spaces," *IEEE Transactions on Microwave Theory and Techniques*, Vol. 53, No. 5, 1613–1623, May 2005.
2. Itoh, T. and A. A. Oliner, "Special issue on metamaterial structures, phenomena, and applications," Guest Editors, "Guest editorial," *IEEE Transactions on Microwave Theory and Techniques*, Vol. 53, No. 4, 1413–1417, IETMAB, Apr. 2005.
3. Jarem, J. M., "Rapidly-convergent, mixed-partial derivative boundary condition Green's function for an anisotropic half-space: Perfect conductor case," *Progress In Electromagnetics Research*, PIER 67, 39–112, 2007.
4. Jarem, J. M., "Resonant frequency analysis of an inhomogeneous, anisotropic, parallelogram cavity using a novel set of mixed-partial derivative boundary condition expansion functions," *Proceedings of the 2007 International Conference on Scientific Computing CSC'07*, 100–105, Jun. 25, 2007.
5. Mesa, F. and F. Medina, "Numerical computation of the space-domain mixed potential Green's functions for planar layered structures with arbitrarily magnetized ferrites," *IEEE Transactions on Microwave Theory and Techniques*, Vol. 52, No. 11, 3019–3025, Nov. 2004.
6. Marqués, R., F. L. Mesa, and M. Horno, "Nonreciprocal and reciprocal complex and backward waves in parallel plate waveguides loaded with a ferrite slab arbitrarily magnetized,"

IEEE Transactions on Microwave Theory and Techniques, Vol. 41, No. 8, 1409–1418, Aug. 1993.

7. Jarem, J. M. and P. P. Banerjee, *Computational Methods for Electromagnetic and Optical Systems*, Marcel Dekker, Inc., Jul. 2000. (Errata: On page 291, after Eq. (5.2.6c) and page 305, after Eq. (5.3.8), $\underline{\underline{K}}$ should be $\underline{\underline{K}} = [iK\delta_{i,i'}]$).
8. Monzon, J. C., "On a surface integral representation for homogeneous anisotropic regions: Two-dimensional case," *IEEE Transactions on Antennas and Propagation*, Vol. 36, No. 10, 1401–1406, Oct. 1988.
9. Zhuck, N. P. and A. G. Yarovoy, "Two-dimensional scattering from an inhomogeneous dielectric cylinder embedded in a stratified medium: case of TM polarization," *IEEE Transactions on Antennas and Propagation*, Vol. 42, No. 1, 16–21, Jan. 1994.
10. Jarem, J. M., "Rigorous coupled wave analysis of bipolar cylindrical systems: Scattering from inhomogeneous dielectric material, eccentric, composite circular cylinders," *Progress In Electromagnetics Research*, PIER 43, 181–237, 2003.
11. Jarem, J. M., "Rigorous coupled wave theory of anisotropic, azimuthally-inhomogeneous, cylindrical systems," *Progress In Electromagnetics Research*, PIER 19, 109–127, 1998. (Errata: On page 115, after Eq. (8) $\underline{\underline{K}}$ should be $\underline{\underline{K}} = [iK\delta_{i,i'}]$).
12. Harrington, R. F., *Time-Harmonic Fields*, McGraw-Hill Book Company, New York, 1961.